A velocity map imaging spectrometer for electron-ion and ion-ion coincidence experiments with synchrotron radiation

D. Rolles[1,2], Z. D. Pešić [1,2], M. Perri[1,2], R. C. Bilodeau[1,2], G. D. Ackerman[2], B. S. Rude[2], A. L. D. Kilcoyne[2], J. D. Bozek[3], and N. Berrah[1]

[1]Physics Department, Western Michigan University, Kalamazoo, MI, 49008, USA

[2]Advanced Light Source, Lawrence Berkeley National Laboratory, Berkeley, CA 94720, USA

[3]Stanford Linear Accelerator Center, Stanford University, CA 94024, USA

Abstract

We have built a velocity map imaging (VMI) spectrometer optimized for angle-resolved photoionization experiments with synchrotron radiation (SR) in the VUV and soft x-ray range. The spectrometer is equipped with four electrostatic lenses that focus the charged photoionization products onto a position-sensitive multi-hit delay line anode. The use of two additional electrostatic lens elements as compared to the standard design of Eppink and Parker [Rev. Sci. Instrum. **68**, 3477 (1997)] provides better focusing of an extended interaction region, which is crucial for most SR applications. Furthermore, the apparatus is equipped with a second microchannelplate detector opposite to the VMI spectrometer, enabling electron-ion coincidence experiments and thereby mass-resolved ion spectroscopy independent of the time structure of the synchrotron radiation. First results for the photofragmentation of CO_2 molecules are presented.

PACS: 39.30.+w, 33.80.Eh

Keywords: photoionization, fragmentation, imaging, velocity map, coincidence

1. Introduction

Since the introduction of two-dimensional photoion and photoelectron imaging techniques in the late 1980s [1], velocity map imaging (VMI) [2] has become a widely used technique in atomic,

molecular and chemical physics [3]. High collection efficiency and simultaneous detection of particles with different velocity and at all emission angles without the need to rotate the detector makes VMI ideally suited to study angular distributions and kinetic energy release in processes with weak cross sections or in dilute targets. Combined with a coincidence-capable detector, VMI is also a prime choice for electron-ion and ion-ion coincidence experiments [4,5].

While still mostly used in conjunction with lasers, the VMI technique has, in recent years, also become popular for use with synchrotron radiation (SR) [5,6,7] and VUV radiation obtained by discharge lamps [4].

However, characteristic differences between the properties of SR and laser light require some modifications to the standard VMI design that we have incorporated into our apparatus:

- The accessibility of higher photon energies with SR sources requires spectrometers that are able to image particles with a higher kinetic energy, which can be achieved by increasing the size of the position sensitive detector, by biasing the drift tube to reduce flight times, and/or by using additional focusing lenses.
- The larger focal length of most SR beamlines compared to common laser sources leads to a more extended interaction region even when using a skimmed molecular beam target, but especially when combined with an effusive gas jet or when operating at high chamber background pressure. Such extended interaction region requires better velocity focusing than achievable with the original two-lens design by Eppink and Parker [2], and additional lens elements have to be introduced.
- Finally, the quasi-cw nature of SR in the typical multi-bunch operation mode of most storage rings requires either pulsed extraction fields or, as in the present case, the use of electron-ion coincidences in order to determine fragment ion masses via the ion time-of-flight.

The following section describes in detail the design of our coincidence apparatus and data acquisition system, while data analysis procedures and exemplary results for the photofragmentation of CO_2 are presented in section 3.

2. Apparatus

In a velocity map imaging spectrometer, electrons or ions created in the interaction area are focused onto a position-sensitive detector by a set of open electrostatic lenses [2]. The lens voltages are chosen such that particles with equal momentum vectors (i.e. equal kinetic energy and emission direction) hit the anode at the same position independent of their starting point. The impact position on the detector thus provides the particles' momentum in the directions parallel to the detector surface. When operated as an ion spectrometer, the ion time-of-flight can also be measured simultaneously in order to determine the kinetic energy and angular distribution for each specific fragment.

Our coincidence apparatus consists of a VMI spectrometer that can be operated either as electron or ion spectrometer, depending on the lens and detector voltages, opposite to a micro-channel plate (MCP) detector for detection of the particles with opposite charge (i.e. electrons, when the VMI is operated as an ion spectrometer, or ions, when the VMI is used to detect electrons). In the following, we will limit the discussion to the case where the VMI is used as an ion spectrometer, and electrons are detected in the opposing MCP detector.

The interaction region, defined by the intersection of a gas jet (either from an effusive gas needle or a molecular beam) with SR from the undulator beamlines 8.0.1 or 10.0.1 of the Advanced Light Source, is situated between the open extractor and a copper-mesh repeller electrode (see Fig. 1). An electrostatic potential of +2000V on the repeller and +1500V on the extractor forces all photo- and Auger electrons onto the double-stack MCP detector, whose front is floating

+100V above the repeller voltage. At the same time, the positively charged ions are extracted in the opposite direction, where they are focused by two additional lenses with potentials of +1000V and -1000V, and, after traveling through a drift tube at -1000V, are detected on a 80 mm position-sensitive hex-anode delay line detector purchased from Roentdek [8]. The lens voltages are chosen such that velocity map focusing is obtained for the ions, and they can be scaled according to the required maximum kinetic energy to be detected. A suitable set of voltages can be found by trajectory simulations with SIMION and/or by experimentally adjusting the voltages until ions with (almost) zero kinetic energy, such as molecular parent ions, are focused to the smallest possible spot in the center of the anode. The negative potential on the 4^{th} lens and the drift tube only needs to be applied when the ion time-of-flight needs to be shortened in order to be able to detect ions with a higher maximum kinetic energy or with extremely different mass to charge ratio in a given detection window.

When operating the apparatus in an electron-ion coincidence mode, a valid coincidence event for the coincidence between an electron and a single ion consists of a total of 8 signals: an MCP timing signal of the electron detector, an MCP timing signal of the ion detector, and 6 position signals from the delay line anode, two from each of the three individual wires. The hexagonal anode design uses three pairs of delay-line wires instead of the two pairs typically used in square-type delay-line anodes in order to provide redundancy, thereby increasing its multi-hit capability [8] to allow simultaneous detection of fragments with equal mass-to-charge ratio.

All eight signals are amplified, discriminated and fed into an 8-channel time-to-digital converter (TDC) card. The TDC card, also purchased from Roentdek, provides a 0.5 ns timing resolution and allows up to 16 hits per channel. In our typical multi-bunch operation, the ion MCP signal provides the common start for the TDC, while the six delay line signals provide the stops from which the anode image can be reconstructed, and the delayed electron MCP signal and a second

ion MCP signal provide additional stops from which the (inverted) ion time-of-flight and the timing of subsequent ion hits can be obtained. For each event, all TDC outputs are stored in a listmode file, which allows analysis of the data event by event.

3. Results

As a first test case for our new apparatus, we chose the photofragmentation of CO_2 molecules after inner-shell excitation, one of the typical showcases for three-body fragmentations [9,10,11]. Fig. 2 shows an ion time-of-flight spectrum for the photoionization of CO_2 at $h\nu$ = 290.7 eV (C 1s -> π^* transition) together with the corresponding anode patterns for each fragment. Ions created with (almost) no initial kinetic energy, such as the molecular parent ions CO_2^+ and CO_2^{++}, are focused to a small spot at the center of the anode, while ions with a given, non-zero kinetic energy resulting from a molecular fragmentation create a circular anode pattern. The angular distribution of the fragment ions is directly visible in the anode patterns.

Since the anode patterns are 2-dimensional projections of a 3-dimensional momentum sphere, ions that are emitted at a non-zero angle with respect to the surface of the detector are superimposed on ions emitted parallel to the detector but with a smaller velocity, creating a somewhat washed out image rather than the desired, well separated angular pattern. The latter can be reconstructed by a so-called "onion-peeling" algorithm [12] or by using the time of flight in combination with the position information to reconstruct the full 3D momentum distribution [13].

Owing to the multi-hit capability of our detector, we can further differentiate the ion distributions according to different decay channels represented by different ion pairs detected in coincidence. Fig. 3 shows the anode pattern for all CO^+ ions compared to CO^+ ions detected in coincidence with an O^+ ion. The striking difference between these two patterns illustrates the additional information that can be obtained by combining VMI and coincidence techniques. While the CO^+ -

O^+ fragmentation channel leads to CO^+ ions with a well defined kinetic energy and angular distribution, both are washed out in the image containing all CO^+ ions. The latter is a combination of the CO^+ - O^+ fragmentation channel together with all processes that lead to the formation of a CO^+ ion together with a neutral fragment.

Besides providing the means for this additional differentiation, the coincident detection of all charged photoionization fragments also allows the determination of the vector, or angular correlations between fragments as shown in Fig. 4 (a). This polar correlation plot illustrates the emission probability of one of the fragments as a function of angle with respect to the emission direction of the second fragment. In the case of the CO^+ - O^+ fragmentations, the narrow peak around 180° reflects the preferential back-to-back emission of CO^+ and O^+ fragments typical for a two-body Coulomb explosion. In contrast, the three-body fragmentation that leads to C^+ - O^+ coincidences results in a much broader vector distribution in the correlation plot, a signature of the bending that occurs after the photoexcitation [14,15]. While these processes are well know in CO_2 molecules, vector correlations can yield further insights into the fragmentation dynamics and the time scales involved in the formation of short-lived intermediate species [16], which are inaccessible to other techniques.

Fig. 4 (b) shows the ion angular distribution of the C^+ fragments measured in coincidence with O^+ fragments. The data are fitted to extract the asymmetry parameter β, given, in the dipole approximation, by the expression

$$\frac{d\sigma}{d\Omega} = \frac{\sigma}{4\pi}\left(1 + \beta P_2(\cos\Theta)\right),$$

where σ is the partial cross section and $P_2(\cos\Theta)$ is the second-order Legendre polynomial that contains the angle θ between the velocity vector of fragment ion and the polarization direction. The fragment ion angular distribution carries information about the symmetry of the excited state

and reaches an asymptotic value of -1 for "perpendicular", i.e. Σ to Π, transition, and +2 for the "parallel transitions" (i.e. Σ state to Σ state). These asymptotic values representing maximum anisotropy are only reached if the fragmentation occurs faster than the rotation of the molecule - a situation know as "axial recoil condition". Even in that case, the ion angular distribution for triatomic molecules can be more isotropic if the excited state is bent, as is the case for the C 1s -> π^* transition in CO_2 [14].

4. Conclusions

Our new velocity map imaging coincidence apparatus is optimized for electron imaging as well as for mass-selective fragment ion imaging in synchrotron-based photoionization studies. If operated in an electron-ion coincidence mode, where ion and electron detection serve as a start and stop signal respectively for a time-to-digital converter (TDC), it enables time-of-flight measurements independent of the time structure of the synchrotron radiation. The use of four electrostatic lenses instead of two provides better velocity focusing compared to standard VMI spectrometers. In combination with a multi-hit capable delay line anode, our spectrometer allows the determination of the kinetic energy release and ion angular distributions for several ions in coincidence as well as vector correlations between the photoionization products. These advanced capabilities can be exploited in order to study the fragmentation dynamics of molecules and clusters after valence and core photoionization.

Acknowledgements

This work was supported by the US Department of Energy, Office of Science, Basic Energy Sciences, Chemical Sciences, Geosciences and Biosciences Division. DR is grateful to the Alexander von Humboldt foundation for support through the Feodor Lynen program. We also

gratefully acknowledge help and advice from Timur Osipov while familiarizing ourselves with the operation of the delay line anode.

References

[1] D. W. Chandler and P. L. Houston, J. Chem. Phys. **87** (1987) 1445.

[2] A.T. J. B. Eppink and D. H. Parker, Rev. Sci. Instrum. **68** (1997) 3477.

[3] A. G. Suits and R. E. Continetti, *Imaging in Chemical Dynamics* (American Chemical Society, Washington, D.C., 2000).

[4] M. Takahashi, J. P. Cave, J. H. D. Eland, Rev. Sci. Instrum. **71** (2000) 1337.

[5] G. A. Garcia, L. Nahon, C. J. Harding, E. A. Mikajlo, I. Powis, Rev. Sci. Instrum. **76** (2005) 053302.

[6] D. S. Peterka, M. Ahmed, C.-Y. Ng, A. G. Suits, Chem. Phys. Lett. **312** (1999) 108.

[7] Y. Hikosaka and E. Shigemasa, J. Electron Spectrosc. Relat. Phenom. **148** (2005) 5.

[8] O. Jagutzki *et al.*, IEEE Trans. Nucl. Sci. **49** (2002) 2477.

[9] K. Okada, H. Yoshida, Y. Senba, K. Kamimori, Y. Tamenori, H. Ohashi, K. Ueda, T. Ibuki, Phys. Rev. A **66** (2002) 032503.

[10] N Saito, A. De Fanis, K Kubozuka, M. Machida, M. Takahashi, H. Yoshida, I. H. Suzuki, A.Cassimi, A. Czasch, L. Schmidt, J. Phys. B **36** (2003) L25.

[11] J.Adachi, N. Kosugi, A. Yagishita, J. Phys. B **38** (2005) R127.

[12] S. Manzhos and H.-P. Loock, Comp. Phys. Commun. **154** (2003) 76.

[13] S. Hsieh and J. H. D. Eland, J. Phys B **29** (1996) 5795.

[14] J. D. Bozek, N. Saito, I. H. Suzuki, Phys. Rev. A **51** (1995) 4563**.**

[15]Y. Muramatsu, K. Ueda, N. Saito, H. Chiba, M. Lavollée, A. Czasch, T. Weber, O. Jagutzki, H. Schmidt-Böcking, R. Moshammer, U. Becker, K. Kubozuka, I. Koyano, Phys. Rev. Lett. **88** (2002) 133002.

[16] S. Hsieh and J. H. D. Eland, J. Phys B **30** (1997) 4515.

Figure captions

Fig. 1: Schematic of the VMI coincidence apparatus (not to scale). Electrons and ions are created in the interaction region (IR) by the interaction of the gas target with synchrotron radiation (SR). The repeller electrode is made out of a 90% transmission copper mesh that allows electrons to be detected on a double-stack MCP array. The extractor, together with additional focusing electrodes, focuses the created photoions on a position-sensitive multi-hit delay line detector.

Fig. 2: Ion time-of-flight spectrum for the photoionization of CO_2 at hν = 290.7 eV (C 1s -> π^* transition) together with the corresponding anode patterns for each fragment (light polarization vector is horizontal). The diameter of the anode pattern increases with increasing kinetic energy of the fragment ions.

Fig. 3: Anode patterns for (a) all detected CO^+ ions compared to (b) CO^+ ions detected in coincident with O^+ ions.

Fig. 4: (a) Vector correlation plot for CO^+ and C^+ ions in coincidence with O^+ ions detected in the direction indicated by the arrow at a photon energy of hν = 290.7 eV. The lines represent the emission probability of the fragment ions, obtained by integrating the measured intensity in one degree intervals, as a function of angle with respect to the emission direction of the O^+ ion. (b) Ion angular distribution for C^+ ions detected in coincidence with O^+ ions at hν = 290.7 eV. The solid line is a fit of the measured data (crosses), yielding a value for the angular distribution parameter β of 0.51 +/- 0.01 compared to a value of 0.4 reported for non-coincident C^+ ions [14].

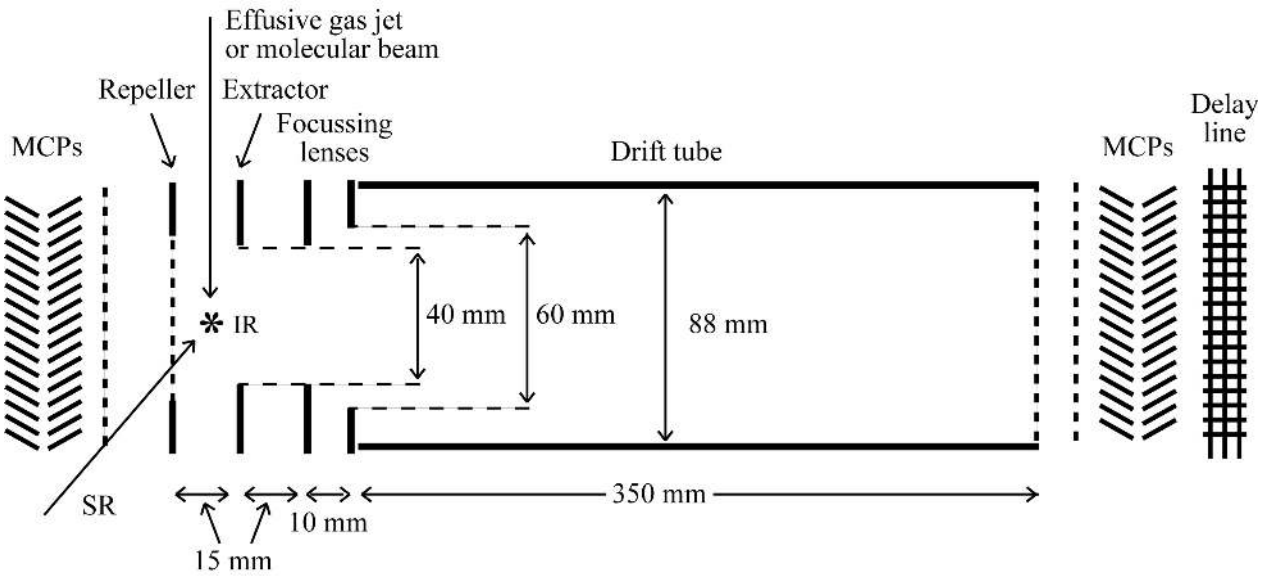
Effusive gas jet
or molecular beam
Repeller
Extractor
Focussing
lenses
MCPs
Drift tube
MCPs
Delay
line
IR
40 mm
60 mm
88 mm
SR
350 mm
10 mm
15 mm

Figure 1

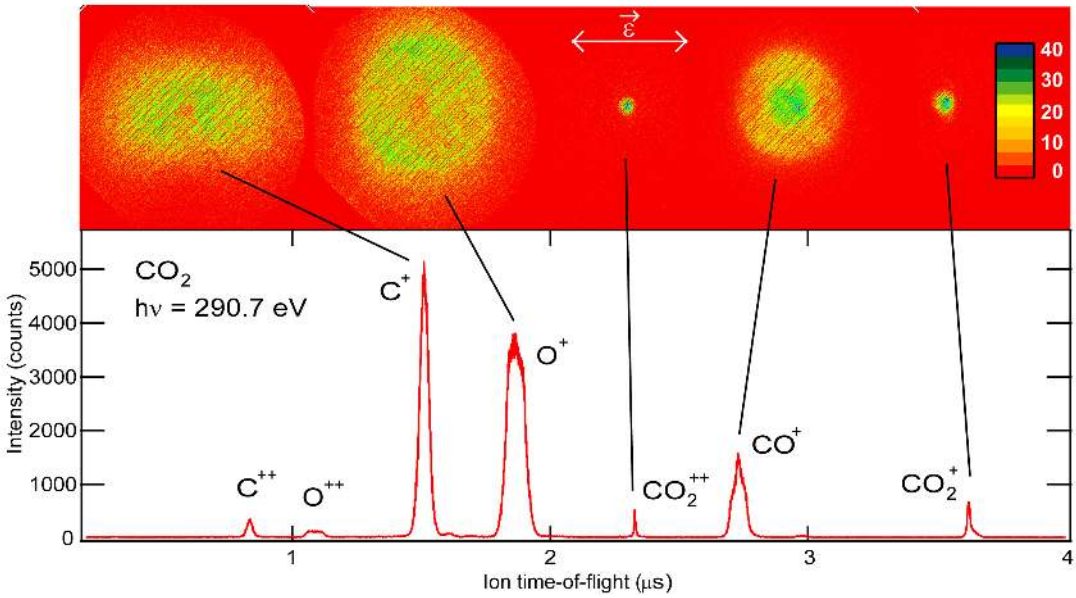
ε
40
30
20
10
0
CO2
hν = 290.7 eV
C+
O+
C++
O++
CO2++
CO+
CO2+
Intensity (counts)
5000
4000
3000
2000
1000
0
1
2
3
4
Ion time-of-flight (μs)

Figure 2

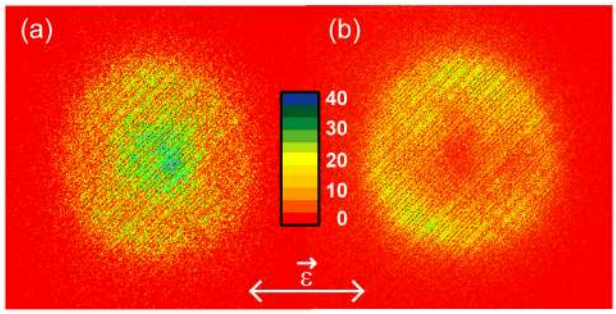

Figure 3

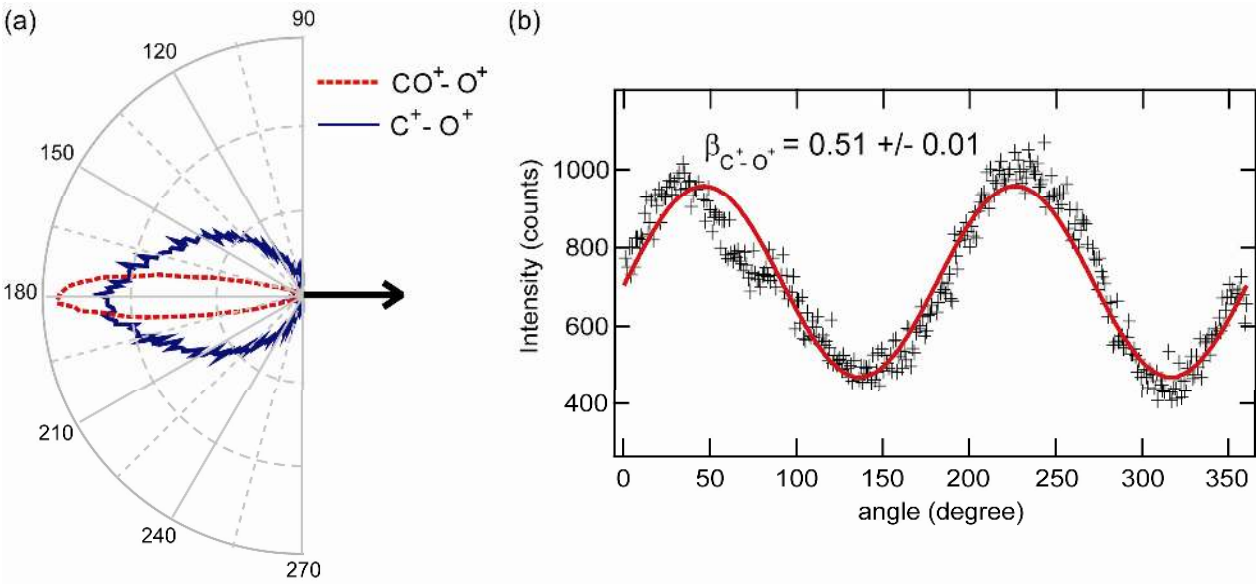
(a)
90
120
150
180
210
240
270
CO+- O+
C+- O+
(b)
βC+- O+ = 0.51 +/- 0.01
Intensity (counts)
1000
800
600
400
0
50
100
150
200
250
300
350
angle (degree)

Figure 4